The International Journal of Advanced Manufacturing Technology (2021) 112:361–373
https://doi.org/10.1007/s00170-020-06387-3

ORIGINAL ARTICLE

Micro milling of additively manufactured AISI 316L: impact of the layerwise microstructure on the process results

Sebastian Greco[1] · Sonja Kieren-Ehses[1] · Benjamin Kirsch[1] · Jan C. Aurich[1]

Received: 3 July 2020 / Accepted: 9 November 2020 / Published online: 19 November 2020

Abstract

In the field of metal additive manufacturing (AM), one of the most used methods is selective laser melting (SLM)—building components layer by layer in a powder bed via laser. The process of SLM is defined by several parameters like laser power, laser scanning speed, hatch spacing, or layer thickness. The manufacturing of small components via AM is very difficult as it sets high demands on the powder to be used and on the SLM process in general. Hence, SLM with subsequent micromilling is a suitable method for the production of microstructured, additively manufactured components. One application for this kind of components is microstructured implants which are typically unique and therefore well suited for additive manufacturing. In order to enable the micromachining of additively manufactured materials, the influence of the special properties of the additive manufactured material on micromilling processes needs to be investigated. In this research, a detailed characterization of additive manufactured workpieces made of AISI 316L is shown. Further, the impact of the process parameters and the build-up direction defined during SLM on the workpiece properties is investigated. The resulting impact of the workpiece properties on micromilling is analyzed and rated on the basis of process forces, burr formation, surface roughness, and tool wear. Significant differences in the results of micromilling were found depending on the geometry of the melt paths generated during SLM.

Keywords Machining · Micromilling · Additive manufacturing · Selective laser melting

1 Introduction

Additive manufacturing (AM) is becoming more and more established in industrial applications. The extended freedom of design of additively manufactured components is combined with a tool-less and near-net-shape production [1]. Producing components without the need for specific tools enables cost-efficient production of small quantities down to batch size one [2]. One of the most used processes for AM of metal parts is selective laser melting (SLM), in which a component is built layer by layer in a powder bed [3]; a layer of new material and defined thickness is applied from a powder supply by a scraper. The cross section of the later workpiece is then exposed by a laser, which melts the powder material and creates the material cohesion. These steps are repeated until the completion of the component [4].

The process parameters used during SLM have a large impact on the material properties of the additively manufactured workpieces [5]. For example, the balling effect may occur as a result of a too high surface tension of the melt in relation to the scanning speed. This results in an unstable melt path, where the powder is not completely melted and is welded onto the surface in a spherical shape [6].

A common material in SLM is the austenitic stainless steel AISI 316L. Due to its biocompatibility, AISI 316L is used in the fields of medicine, e.g., in the fabrication of implants, which are typically customized and represent unique specimens [7]. Due to the increasing complexity of the AM process itself and the increasing demands on the powder properties when additively producing microstructured components in a single process step [8], SLM and subsequent micromilling are a suitable process splitting for structuring surfaces of individually shaped parts in the micrometer range.

The effects of part porosity and building direction on the workpiece properties and the corresponding impact of the workpiece properties on micromilling and its results have

✉ Sebastian Greco
sebastian.greco@mv.uni-kl.de

[1] Institute for Manufacturing Technology and Production Systems, TU Kaiserslautern, Gottlieb-Daimler-Str., 67663 Kaiserslautern, Germany

not been researched yet. A selection of research done on micromilling, machining of AM AISI 316L, and micro-AM is presented below.

In [4], current developments in microadditive manufacturing are given. Gieseke et al. present the SLM of microneedles without any subsequent machining. The additively manufactured structures have a height of 1200 μm with a minimum wall thickness of 100 μm. A structure resolution < 50 μm was achieved. The layer thickness during additive manufacturing was $S_D = 20$ μm; the diameter of the laser focus was 19.9 μm. The powder used had a grain diameter in the range of 5–25 μm [9, 10].

Coelho et al. investigated the surface roughness during micromilling of AM AISI 316L with different feed directions and a two-stage variation of the tool diameter (600 μm, 800 μm). The variation of the feed direction showed an anisotropy of the material by differences in the surface roughness which was reduced by using a larger tool diameter [11].

Kaynak and Kitay have investigated finishing when turning in order to improve the surface properties of additively manufactured components made of AISI 316L. A significant reduction of the surface roughness from 7 ± 1 μm to Ra < 1 μm was achieved. Further, depending on the process parameters used for turning, a hardening of the surface and subsurface was observed. In addition, the porosity of the additive microstructure at the surface and in areas close to the surface was reduced, which results in better fatigue behavior due to reduced crack susceptibility [12].

In the work of Alexeev et al., the effects of feed direction variation during milling in relation to the layer orientation of AM workpieces made of AISI 316L were investigated. Milling tools with a diameter of 12 mm were used. Changing process forces were determined in dependence on the dimensions of the melt paths of the workpiece microstructure. The differences are due to the melt borders resulting from SLM, which prevent deformations of dislocations during milling and thus increase cutting forces [13].

The presented studies showed that the feed direction in relation to the build-up direction has an influence on the finishing of AM workpieces, but do not provide any information on the extent to which these effects apply for micromilling using tools with $d < 50$ μm. Due to the much smaller tool diameters used in this research ($d_{effective} = 50$ μm) and the reduced ratio of layer thickness S_D and tool diameter ($d/S_D = 2$), an increase of the influence of the machining direction is expected due to the microstructure size effect [14], which may result in the material no longer being considered isotropic; this effect has not been investigated for machining AM materials. Further, a difference between micromilling additively manufactured and reference material is expected, as the material production processes are fundamentally different and result in significant variations in the microstructure of the machined materials.

In this paper, the effects of the process parameters and the build-up direction used during SLM on the workpiece properties and the resulting impact of the workpiece properties on micromilling are investigated. In this way, the influence of the AM of the machined materials on the process of micromilling using tools with $d = 50$ μm is described. Therefore, two different parameter sets for SLM, which differ in laser power and scanning speed, are used. The produced parts are characterized with regard to their relative density, roughness, chemical composition, microhardness, and melt path geometry. As they are the most important results of machining processes and are often indispensable for the functionality of the component to be produced, burr formation and the produced surface quality when micromilling are determined. Process forces and tool wear are analyzed for a better understanding of effects occurring during machining. In addition, correlations to the AM process conditions are identified. The results of the parts produced by SLM are also compared to reference workpieces, which were made of casted, rolled, solution-annealed, and water-quenched material.

2 Materials and methods

The present study is divided into additive manufacturing of the parts, characterization of the AM parts, micromilling of the AM and reference parts, and the evaluation and discussion of the process results.

2.1 Additive manufacturing

The parts produced by SLM were built using the Mlab Cusing by Concept Laser[1]. In Fig. 1, the machine and its specifications are shown. This machine is equipped with a 100 W fiber laser

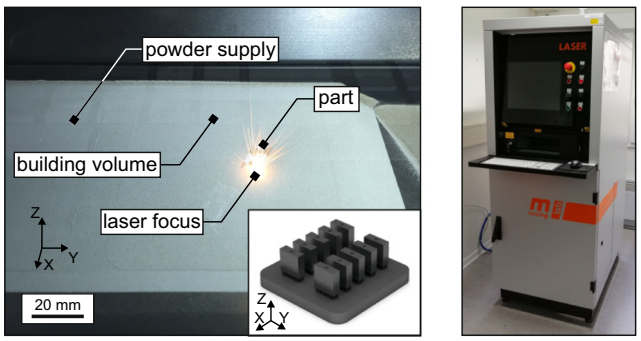

Concept Laser Mlab cusing

building volume: 90 x 90 x 80 mm	focus diameter: ~ 50 μm
layer thickness: 15 - 50 μm	heated building volume: no
max. laser power: 100 W	inert gas: nitrogen
max. scanning speed: 7.000 mm/s	

FBK/033-030

Fig. 1 Building volume during SLM, exterior view of SLM machine, and technical specifications

(Nd:YAG, $\lambda = 1064$ nm, laser beam diameter ~ 50 µm). The building volume comprises 90 × 90 × 80 mm. The dimensions of the additively produced workpieces are 20 × 20 × 7 mm. During SLM, the workpieces' smaller surfaces were positioned parallel to the build platform (*XY*-plane) (see Fig. 1).

In order to characterize the powder used for SLM, the circularity c of the powder particles was calculated according to [15] as:

$$c = \sqrt{\frac{4\pi A}{U^2}} \tag{1}$$

with A corresponding to the projected area of a single powder particle and U to the corresponding perimeter. For an ideally round circle, $c = 1$ applies; for all non-round geometries, $c < 1$ applies. Due to the high circularity of the powder used for SLM in this research (90% of the grains $c > 0.93$), the powder particle's projected area can be assumed as ideally round. Based on this, the particle diameter of the AISI 316L powder was calculated using the equivalent diameter of the particle's projected area.

Figure 2 shows the particle size distribution of the AISI 316L powder used for SLM. The weighted mean particle diameter was $d_{50} = 32$ µm ($d_{10} = 20$ µm, $d_{90} = 45$ µm). In addition, a scanning electron microscope image of the AISI 316L powder is given in Fig. 2, also showing the high circularity of the AISI 316L powder.

Two parameter sets for SLM, already investigated in previous studies [16], were selected for this investigation. They significantly differ in the amount of energy supplied to a specific volume, with AM1 corresponding to the lower energy density and AM2 to the higher one. The reduction of the input energy density E_V and the associated production of the strongly porous microstructure of AM1 allow the investigation of the influence of the workpiece's relative density on micromilling. E_V can be calculated according to [17] as:

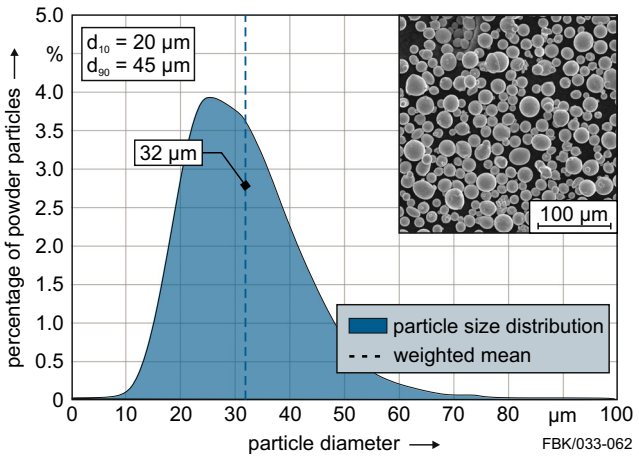

Fig. 2 Particle size distribution and scanning electron microscope image of AISI 316L powder

$$E_V = \frac{P}{v_S * S_D * S_A} \tag{2}$$

with laser power P, scanning speed v_S, layer thickness S_D, and hatch spacing S_A. A detailed overview of the process parameters used during SLM can be taken from Table 1.

2.2 Sample characterization

The roughness of the as-built surface of the AM workpieces was measured using the stylus instrument MarSurf M300 by Mahr GmbH[1]. The relative density ρ of the AM workpieces was calculated as follows:

$$\rho = 100\% * \frac{m}{x \cdot y \cdot z \cdot \rho_{316L}} \tag{3}$$

with the measured mass m; the workpiece dimensions x, y, z; and the density of the material $\rho_{316L} = 7.99$ g/cm^3. The variables were determined by using an electric vernier height gauge (accuracy ± 0.01 mm, BZT Maschinenbau GmbH[1]) for the workpiece dimensions and a precision balance (accuracy ± 0.001 g, KERN & SOHN GmbH[1], EMB 200-3) for the mass. The workpieces used for the determination of the relative density were machined by a conventional milling machine in order to ensure a cubic volume before the measurements.

After determining their volume, the workpieces were separated in their *XY*- and *YZ*-plane (see Fig. 1), ground, polished, and etched for hardness measurements and micrographs. For this purpose, the Mecatech 334 by Presi GmbH[1] was used with a head rotational speed of $n_H = 60$ min^{-1} and working rotational speed of $n = 300$ min^{-1} for down grinding (P1200, P2500, P4000) and $n = 150$ min^{-1} for polishing. The contact force was set to 10 N. When etching, the workpieces were submerged into a Beraha-II solution at room temperature and twirled for 8 s. Immediately after etching, the workpieces were washed with water to stop the chemical reaction.

The cross sections were used to determine the hardness (HV 0.01) of the investigated materials inside the workpieces in order to exclude boundary effects. The hardness was measured using 5 measuring areas (near the edges of the polished

Table 1 SLM parameters

Process parameters	AM1	AM2
Scanning strategy	Successive chessboard	
Layer thickness	25 µm	
Hatch spacing	56 µm	
Laser power	70 W	50 W
Scanning speed	1500 mm/s	300 mm/s
Input energy density	33.3 J/mm^3	119.0 J/mm^3

plane (0.2 mm from each edge) and in the center of the polished plane), each with 4 measurements in both planes (*XY*- and *YZ*-plane). The indicated value of the hardness corresponds to the arithmetic mean of the 40 measured values. The hardness was measured by using the Micromet 5103 by Buehler GmbH[1].

2.3 Micromilling

The micromilling tests were carried out on the micromilling center (MMC), self-developed at our Institute for Manufacturing Technology and Production Systems (FBK) of the TU Kaiserslautern [18]. The desktop machine tool is characterized by a high dynamic response due to low moving masses, yet high stiffness [19].

The effective diameters of the single-edged micromilling tools were 50 µm, the tool orthogonal clearance was 20°, and the tool orthogonal rake angle and helix angle were 0°. They were made of cemented carbide with a grain size of 0.2 µm, 91% WC, and 9% Co. The manufacturing and geometry of the micromilling tools is described in detail in [20]. The machining parameters used during micromilling are based on previous studies investigating the minimum runout of the spindle [21] and the influence of the feed per tooth during micromilling processes [22]. The feed travel was chosen to ensure that the tools show significant tool wear, but are still functional for the purpose of tool wear comparison. The machining parameters are summarized in Table 2.

The feed travel was achieved by 17 parallel arranged grooves with alternating feed directions which extend over the entire width of the workpiece. To study the influence of feed direction relative to the layer orientation of the AM workpieces, two combinations of directions were used. Referring to the coordinate system of the machine, the feed direction was kept constant. In the following, the two investigated combinations are named as feed direction "perpendicular to the build-up direction" (feed direction in workpiece *Y*-direction) and feed direction "parallel to the build-up direction" (feed direction in workpiece *Z*-direction) (see Fig. 3). Thus, not crossing and crossing the AM build-up layers were realized. The workpieces were face milled before micromilling. All experiments were repeated three times.

Table 2 Micromilling machining parameters (side milling)

Machining parameters	Value
Feed travel l_f	340 mm
Feed per tooth f_z	1 µm
Depth of cut a_p	5 µm
Spindle speed n	50,000 min^{-1}

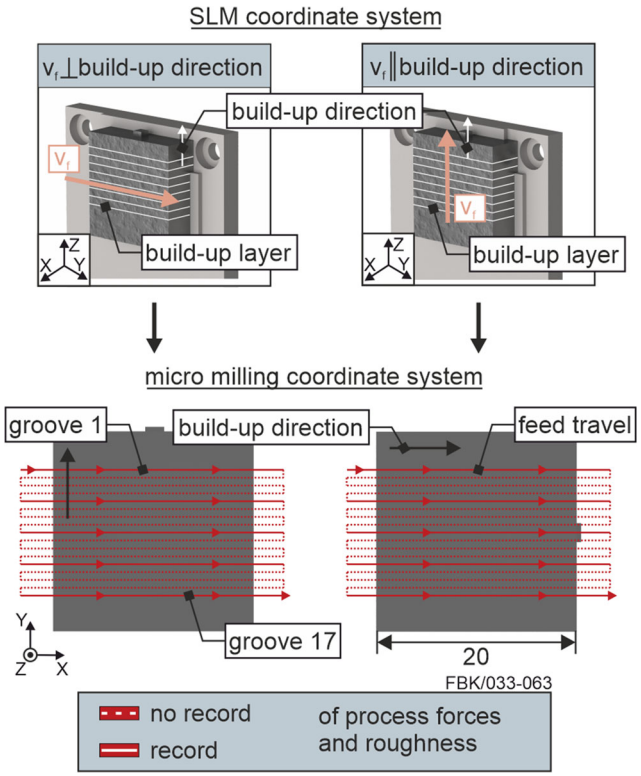

Fig. 3 Feed direction in relation to build-up direction during micromilling and arrangement of grooves on workpiece

2.4 Measurement technology

During the experiments, the forces in the *X*-, *Y*-, and *Z*-direction were measured at constant intervals (see Fig. 3) using a dynamometer (Kistler[1], MiniDyn Type 9119AA1) with a response threshold of < 0.002 N. The force signals were filtered by a bandpass of ± 50 Hz of the spindle's rotational frequency. For each groove (l_f = 20 mm), the process forces were calculated by a vector addition of the averaged root mean square (RMS) of the filtered forces in the *X*-, *Y*-, and *Z*-direction.

The machined surface was optically characterized using a confocal microscope (Nanofocus[1], µsurf OEM) with an objective with ×60 magnification (NA = 0.9, measuring area 260 × 260 µm, resolution in the *Z*-direction 2 nm, resolution in the *X*- and *Y*-direction 0.5 µm). According to the feed per tooth of f_z = 1 µm (see Table 2) and following DIN EN ISO 4288 [23], the measuring path for determining the roughness values of Ra was interpolated as 400 µm. Thus, for roughness determination, confocal microscopy images with a size of 450 × 260 µm were taken, initially after a feed travel l_f = 10 mm and then every 80 mm. The measured data was evaluated with the software µsoft Analysis by Digital Surf[1]. The arithmetic average profile roughness Ra was evaluated in the middle of the micromilled grooves in feed direction using a Gaussian filter of λ_c = 8 µm. For the determination of the arithmetical mean height of the scale limited surface Sa and the maximum pit height of the scale limited surface Sv, a

measuring field of 40 × 400 µm was used. During the determination of Sa, the measuring field was further reduced where necessary so that the analyzed surface was free of pores and only reflects the roughness created during micromilling.

Due to the small dimensions and the susceptibility to errors in the quantitative evaluation of these, tool wear and burr formation were evaluated solely qualitatively. Images of the micromilled grooves and the micromilling tools were taken by the scanning electron microscope (SEM) XL40 by Philips[1]. In addition, the energy dispersive X-ray spectroscopy (EDS) integrated in the SEM was used to determine the chemical composition of the AM and the reference workpieces.

The uncertainty of the measurements is often given by the mean standard deviation $\overline{\sigma}$. To determine the mean standard deviation, the standard deviation was first calculated based on the three repetitions of each examination at identical points. Then, the arithmetic mean of these standard deviations for a given material or combination of material and feed direction was calculated.

3 Results and discussion

In order to link the influence of additively manufactured workpieces on micromilling, the following section is divided into the characterization of the AM workpieces and the results of micromilling.

3.1 Characterization of AM workpieces

Figure 4 shows the results of the characterization of the workpieces AM1 and AM2.

The microstructure of AM1 showed large pores, which is also evident from the relative density of $\rho = 79.0\%$ ($\sigma_\rho = 1.3\%$). The hardness of AM1 was 258 ± 12 HV 0.01 which is much higher than the hardness of the reference material (218 ± 17 HV 0.01 [24]). The roughness of the as-built AM1 surface was Ra = 7.4 µm ($\sigma_{Ra} = 7.6\%$). The determined roughness Rz = 42 µm ($\sigma_{Rz} = 7.3\%$) was within the range of the powder grain diameter of the raw material used.

The microstructure of AM2 was almost free of pores and the determined relative density was $\rho = 95.7\%$ ($\sigma_\rho = 0.7\%$). AM2 was, with 267 ± 7 HV 0.01, the hardest workpiece studied in this paper. The as-built surface of the AM2 workpiece showed a roughness of Ra = 8.8 µm ($\sigma_{Ra} = 9.0\%$) and a determined roughness of Rz = 44 µm ($\sigma_{Rz} = 8.1\%$).

The comparatively low relative density of AM1 is due to the lower input energy density of 33.3 J/mm^3 compared to 119.0 J/mm^3 at AM2. Due to the very high scanning speed during the generation of AM1, the time available to completely melt the corresponding powder volume is not sufficient, despite increased laser power. Especially, powder grains with larger diameters require a higher amount of energy to be heated above their melting temperature [25], which is not fully achieved at lower input energy density. Some powder particles are not melted at all and can be seen as spherical structures in the micrograph of AM1.

The process parameter combination used for the SLM of AM2 is much more qualified to create a homogenous

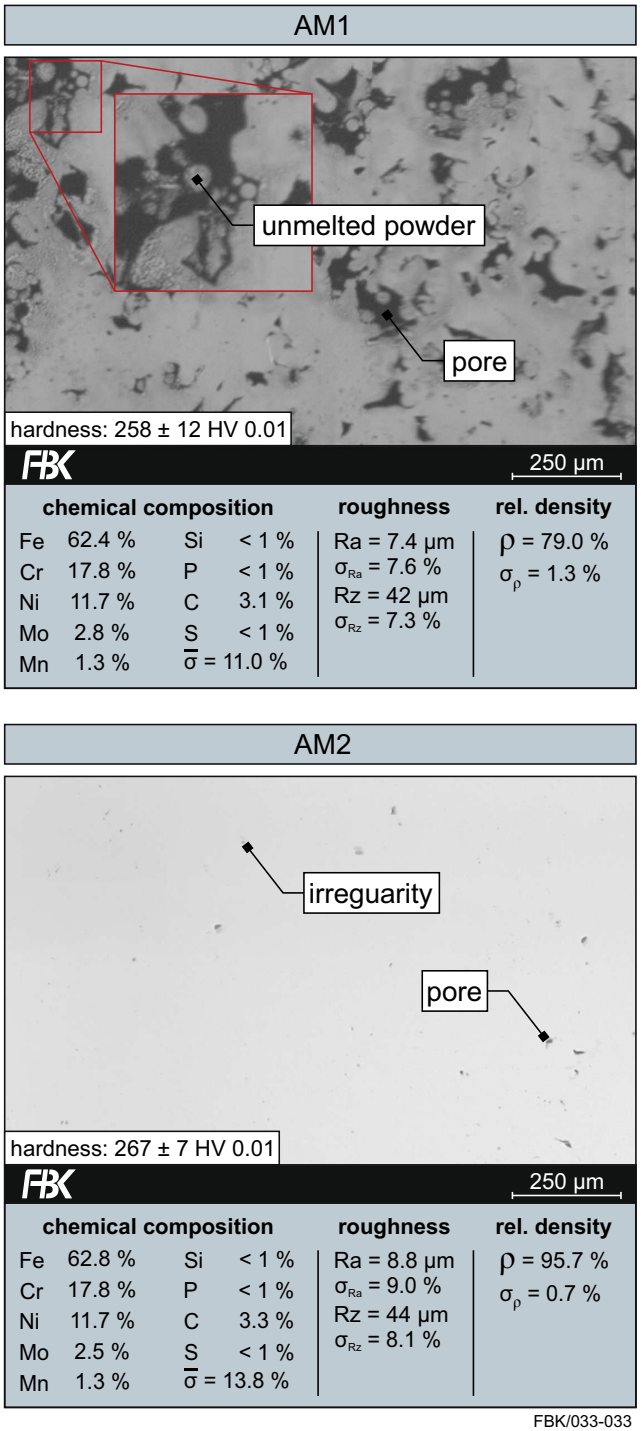

Fig. 4 Characterization of AM1 and AM2 showing the micrograph, chemical composition, surface roughness of the as-built surface, and relative density

workpiece. The remaining small pores are due to evaporation [26] and cavitation [27, 28] of the melted powder, which occurs if the input energy is too high.

The higher hardness of AM workpieces compared to the reference material is already known from literature [29] and is due to the directed microstructure, characteristic for AM.

Both AM1 and AM2 show approximately the same roughness at the as-built surface. This is due to partly melded powder grains at the border of the just-lasered build-up layers during SLM (see Fig. 3, workpiece positioning). Due to decreasing temperatures with increasing distance to the laser-exposed powder spot in the workpiece's *XY*-plane, powder grains located next to the perimeter of the build-up layers are always only partially melted and thus fixed to the workpiece. As the temperature always decreases with distance to the melt path and thus the melting temperature of the powder will not be reached any more at a given point, this effect is detached from the energy input. Therefore, the powder particle size dictates the roughness of the workpiece surfaces perpendicular to the build-up layers.

Since columnar grains can grow over several melt paths in SLM materials [30, 31] and especially microstructure effects have an influence on micromilling processes [32, 33], the geometry of the melt paths is focused in this paper. Figure 5 shows the etched surfaces of separated AM1, AM2, and reference workpieces (*YZ*-plane). The build-up direction of the additively manufactured workpieces can be determined by the scaly shape of the melt paths. The melt path shapes are due to the heat transfer into surrounding powder and the already build workpiece. The micrograph of AM2 clearly illustrates the layered build-up characteristic for AM with individual melt paths resulting from the laser exposure. The shown melt borders are caused by the solidification of individual melt paths. The melt path width w and the melt path height h are exemplary illustrated on AM2 which consists of mainly non-porous connected melt paths. For AM1, the average ratio of melt path width to melt path height was determined as $w/h = 1.47 \pm 0.27$, and for AM2, $w/h = 2.15 \pm 0.63$. The averaged dimensions of the melt paths ($\overline{\sigma}$ = 22.9%) are as follows: $w_{AM1} = 73$ µm, $h_{AM1} = 51$ µm, $w_{AM2} = 84$ µm, and $h_{AM2} = 41$ µm.

AM1 is also showing melt path characteristic for SLM workpieces; however, the microstructure contains pores of the same scale as the melt paths. When analyzing the micrograph of the reference material, a typical austenitic structure with characteristic twin boundaries can be seen.

3.2 Micromilling results

The following section shows the results of micromilling AM1, AM2, and the reference material regarding process forces, surface roughness, tool wear, and burr formation.

3.2.1 Tool Wear

Figure 6 shows the SEM images of the micromilling tools used for machining AM1, AM2, and the reference material after a feed travel of $l_f = 340$ mm.

Significant differences can be observed in terms of type and degree of the tool wear depending on the machined material and the feed direction relative to the layer orientation of the workpieces. In general, AM1 shows less tool wear compared to AM2 and the reference material. Since the micromilling tools are equipped with only a single cutting edge, the entire machining is performed as interrupted cut. Per tool rotation, the cutting edge is entering and leaving the material once. The influence of additional material entries and exits when micromilling through pores is therefore negligible. However, the reduced tool wear can be explained by the lower material removal caused by the low relative density of AM1 ($\rho = 79.0\%$) compared to AM2 ($\rho = 95.7\%$) and the reference material ($\rho = 100.0\%$).

There is also a clear influence of the feed. In the case of AM1 and AM2, a higher wear results when micromilling parallel to the build-up direction. This influence is attributed to the anisotropic material structure, characteristic for workpieces manufactured by SLM. According to Hall-Petch strengthening, dislocations accumulate along grain

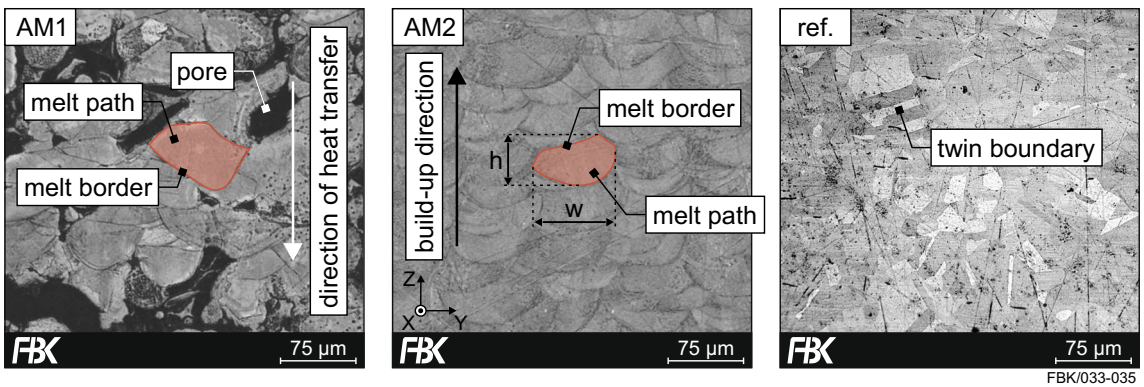

Fig. 5 Etched microsection of AM1, AM2, and reference material (ref.) and indication of build-up direction and direction of heat transfer

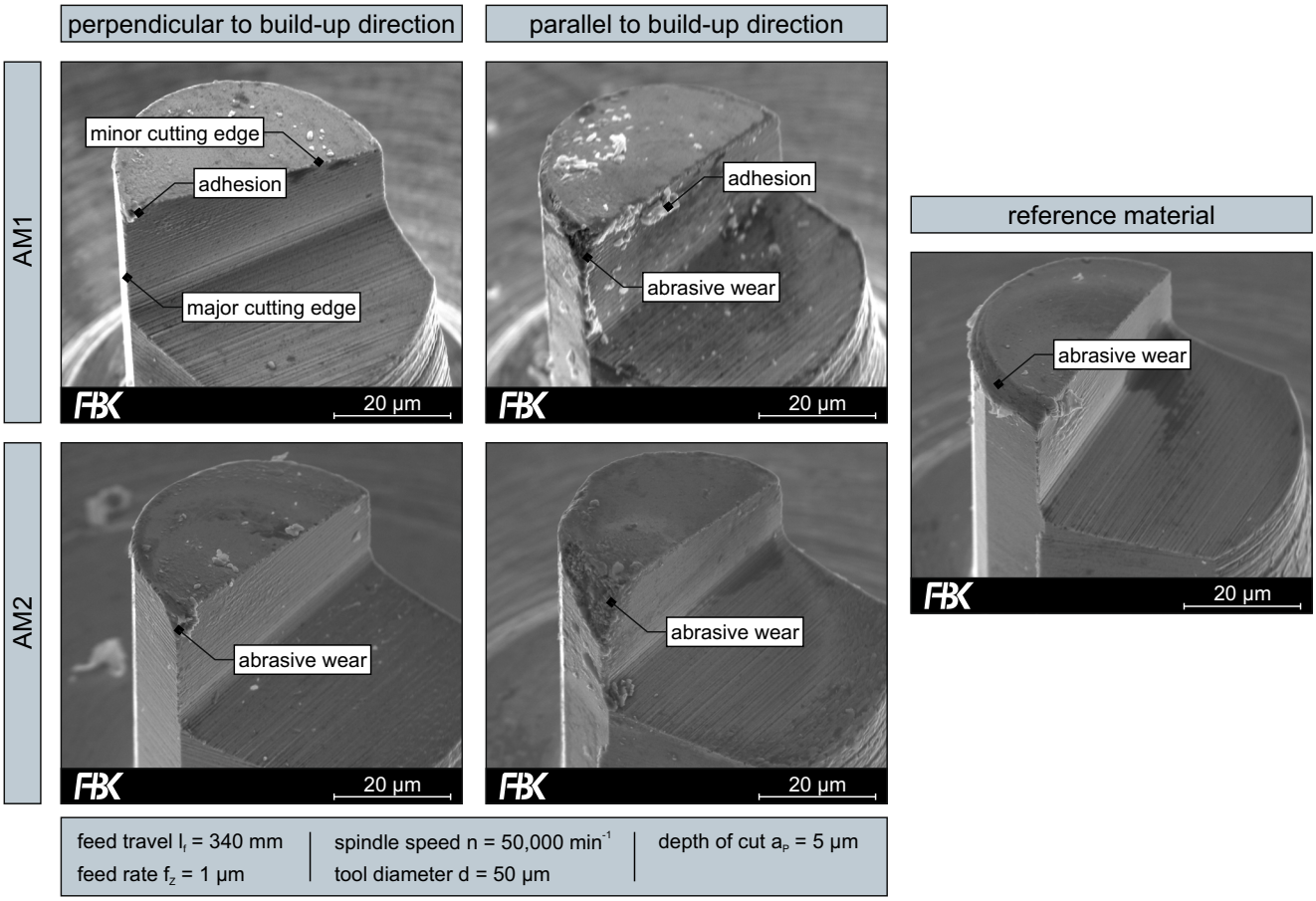

Fig. 6 Representative tool wear of micro end mills after machining AM1, AM2 with feed direction perpendicular and parallel to the build-up direction, and reference material

boundaries [34] which are comparable to melt borders. As a result, during machining, the dislocations in the material are moved towards the melt borders where they accumulate. This accumulation increases the likeliness that dislocations are hindered in their movement [35], which in turn leads to a strengthening of the material and increased tool wear when crossing the melt borders. Due to the ratio of melt path width w to melt path height h (see Fig. 5) of 1.47 ± 0.27 (AM1) and 2.15 ± 0.63 (AM2), the increased tool wear when micromilling with feed direction parallel to the build-up direction can presumably be attributed to the increased crossing of melt borders. Conversely, when milling with feed direction perpendicular to the build-up direction, dislocations are moved over a longer distance due to the ratio of w/h and fewer melt borders are crossed, resulting in a more stable load condition and therefore less tool wear.

When micromilling the reference material, tool wear mostly occurred on the circumferential edge between the peripheral flank face and the radial flank face (facet clearance) of the micro end mill. Since the tool wear when micromilling reference material significantly differs from that of AM workpieces, a different material behavior during material separation can be assumed. This difference in material behavior between AM and reference workpieces is also illustrated by considering the process forces.

3.2.2 Process forces

Figure 7 shows the process forces during micromilling for all experimental repetitions of each material and feed direction. Due to the detailed depiction of all repetitions (marked as _1, _2, _3), special aspects in the force signal of individual tools, such as the formation of build-up edges, can be identified. Since the process forces were calculated as average values of each groove, the values of feed travel of the process forces correspond to the respective groove centers (see Fig. 3).

There are significant differences in the process forces of the materials AM1, AM2, and the reference material. AM2 shows a dependency on the feed direction during micromilling whereas AM1 seems to be unaffected by the feed direction. Micromilling of the reference material achieves the highest process forces with 0.29 N. Within the considered feed travel, the process force of AM1 is comparatively stable compared to the forces of the reference material. Micromilling of AM2

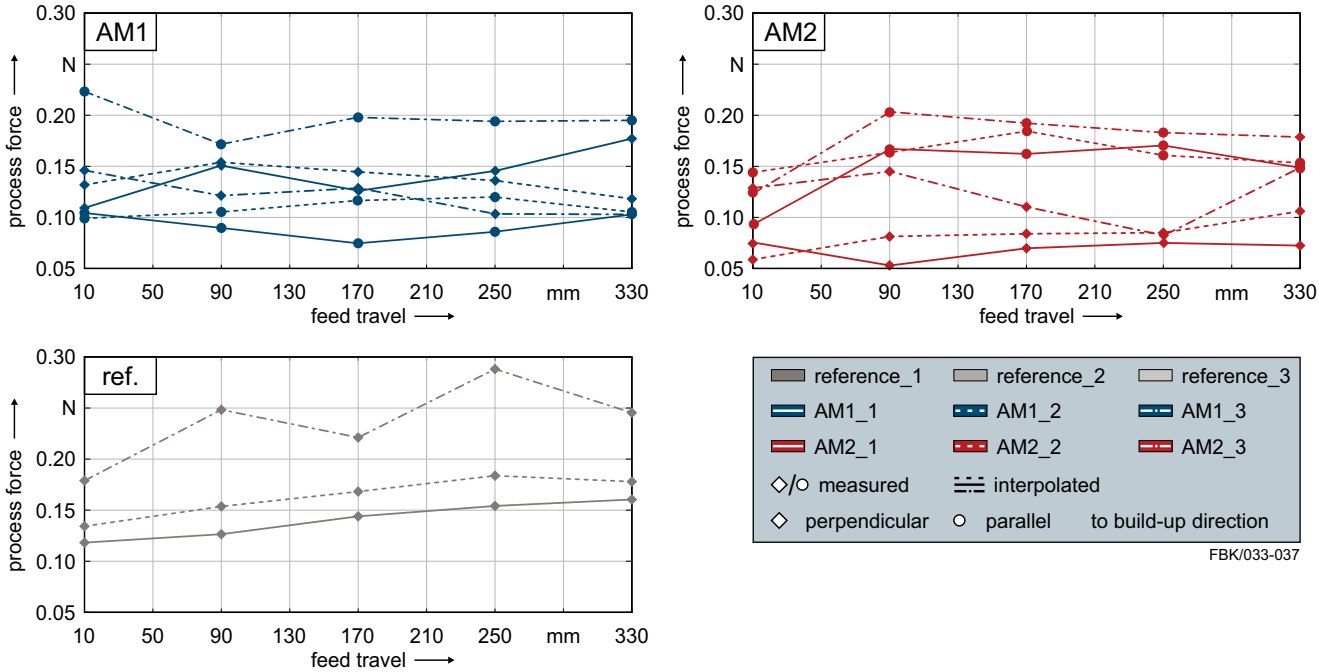

Fig. 7 Process forces of AM1, AM2, and reference material

perpendicular to the build-up direction reaches the lowest forces whereas micromilling AM2 parallel to the build-up direction has process forces up to 0.2 N.

In two of the three experimental runs, the process forces of the reference material increase constantly, indicating continuous wear during micromilling. In contrast, reference_3 shows generally larger process forces as well as some local increases and decreases of the process force. These are due to the formation of built-up edges and their rip-off during machining. Ignoring the two local peaks of reference_3, a similar linear increase as in reference_1 and reference_2 can be observed.

The process forces of AM2 machined perpendicular to the build-up direction are reasonably constant which is an indicator of only slight tool wear during machining. This low tool wear is equivalent to a reduced amount of cutting edge rounding and can also be seen in Fig. 6. In general, higher process forces can be seen during machining of AM2 with feed direction parallel to the build-up direction. In addition, an increase in the process forces of AM2 is observed at the beginning of the feed travel. This is due to the formation of a built-up edge which is ripped off and results in an increased cutting edge radius. Therefore, due to the initial formation of built-up edges, AM2 reaches similar process forces at l_f = 90 mm as the continuously wearing tools used for the reference material at l_f = 330 mm. The differences in process force when micromilling AM2 parallel or perpendicular to the build-up direction may be due to the Hall-Petch strengthening. This increasingly occurs when machining parallel to the build-up direction as a result of the ratio of $w/h > 1$. Thus, the increased process force during machining AM2 parallel to the build-up direction compared to perpendicular to the build-up direction is due to the increased crossing of melt borders with locally accumulated dislocations superimposed by the formation of build-up edges. Analogously, the lower process forces during machining AM2 perpendicular to the build-up direction are attributed to the reduced crossing of melt borders, leading to lower tool wear and thus resulting in lower cutting edge radii.

The process forces of AM1 ranges between 0.07 and 0.23 N. When micromilling AM1, no influence of the relation between feed direction and build-up direction can be determined. Since the ratio of w/h for AM1 is reduced compared to AM2, this non-existent correlation between feed direction and build-up direction is due to the microstructure of AM1. The closer to one ratio of w/h indicates a more even formation of the length and width of the melt paths, which leads to a similar amount of melt border crossing during machining independent of the feed direction. The comparison of process forces of AM workpieces shows the following order in increasing direction: AM2 machined with feed direction perpendicular to the build-up direction, AM1 independent from feed direction, and AM2 machined parallel to build-up direction. Despite a significantly lower amount of material removal when machining AM1, the process forces of AM1 are slightly higher than those of AM2 machined perpendicular to the build-up direction. This may be a result of the number of crossed melt borders as well. The averaged values for melt path width and length of AM1 are both within the values of AM2 ($w_{AM2} > w_{AM1} > h_{AM1} > h_{AM2}$). Consequently, the number of crossed melt borders during micromachining AM1 regardless

of the feed direction lies between those of AM2 machined with feed direction perpendicular and parallel to the build-up direction. In summary, since the process force is related to the number of melt border crossings due to the accumulations of dislocations at melt borders, the different levels of process forces of AM1 and AM2 are based on the microstructure of the material defined during AM and the feed direction during machining.

3.2.3 Surface roughness

Figure 8 depicts the results of the characterization of the micromilled surfaces based on the values of Ra, Sa, and Sv for all materials and feed directions.

Considering Fig. 8a and b, the mean values of Ra are very similar for AM1 and the reference material. However, AM1 exhibits the highest values of roughness. Just as with the process forces, AM1 shows no dependency of the roughness on the combination of feed direction and layer orientation. The lowest roughness was achieved when machining AM2. Similarly, no significant difference in the roughness of the milled surface depending on the feed direction was found after $l_f = 170$ mm, whereas, at the beginning of the feed travel, noticeably higher roughness was observed when micromilling parallel to the build-up direction compared to micromilling perpendicular to the build-up direction. These initially increased values of Ra are also reflected in different values and standard deviations for AM2 given in Fig. 8b.

The higher values of roughness for AM1 are again partially a result of the comparatively porous structure (see Fig. 4). Some of the pores on the surface are closed by plastic deformation during machining [19]. However, due to the high number of pores in AM1 workpieces and the large ratio of cross section of undeformed chips to pore size of AM1 during micromilling, this effect of pore closure cannot eliminate all pores, which leads to surface defects at the groove bottom. These surface defects are also indicated in Fig. 8d, which shows the maximum pit height Sv for AM1, AM2, and the reference material. Due to the increased number of open pores and their depth, Sv of AM1 is significantly increased. The shown maxima of AM1 clearly reveal the presence of pores at the surface of the micromilled grooves. For this reason, the roughness of the surfaces located inside of pores (measuring path = 43.7 ± 14.5 µm) was compared with that of the directly surrounding groove bottom of AM1 workpieces (measuring path = 38.0 ± 0.9 µm). The comparison of these roughnesses determined an increase in roughness by factor 7.2 ± 1.1 between pore and groove surfaces. Thus, the increased roughness of AM1 workpieces can be attributed to the higher number of open pores and their increased roughness resulting from the comparatively high porosity of the machined material.

AM2 workpieces contain less pores (see Fig. 4). For AM2, the same mechanisms and geometric conditions apply as they do for AM1, but due to the smaller number of existing pores in general, less open pores are present at the groove bottom. This fact is emphasized by comparing the values of Sv and their corresponding maxima for AM1 and AM2 in Fig. 8d. The lower roughness comparing AM2 and AM1 workpieces is hence a result of the increased relative density of AM2. This effect of closing pores at the workpiece surface and the increased roughness of pores is superimposed by the differences in tool wear of the micromilling tools (see Fig. 6). The varying

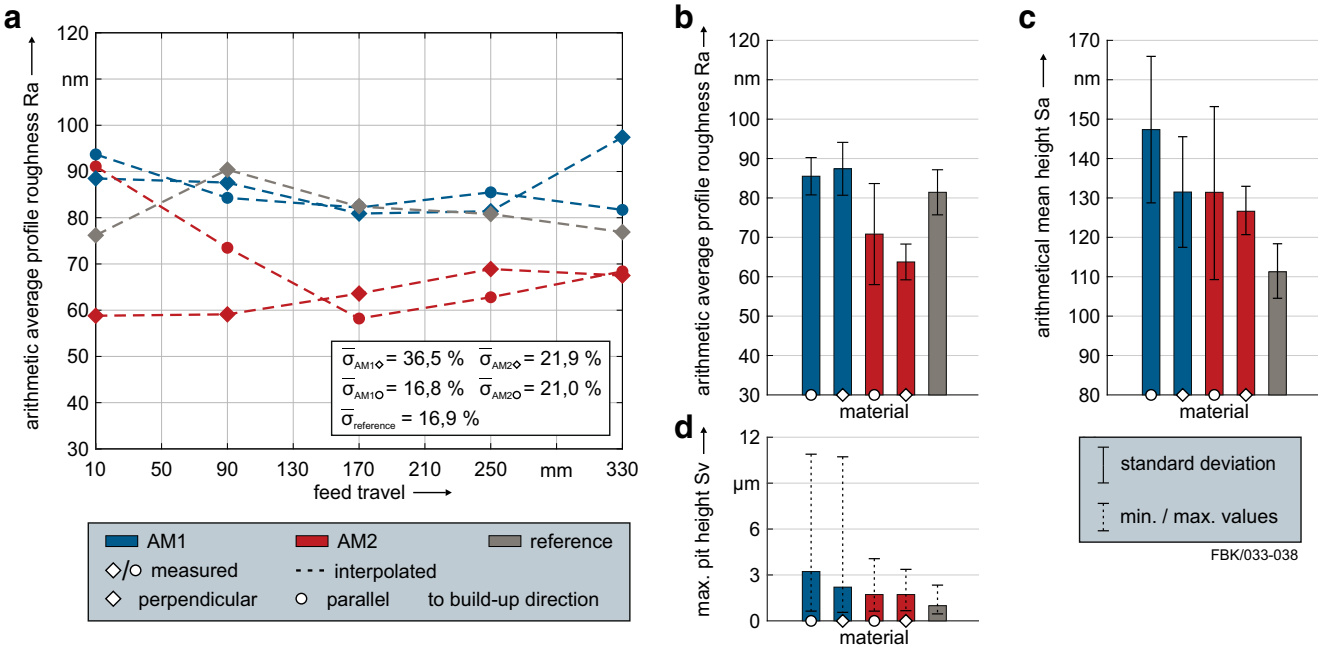

Fig. 8 Surface roughness depending on material and feed direction. **a** Ra over feed travel. **b** Ra. **c** Sa. **d** Sv

degree of tool wear leads to changing cutting edge radii. The increased wear of the cutting edge of the micromilling tools used for AM2 leads to a lower kinematic roughness at the groove bottom, which thus results in the reduced measured arithmetic average profile roughness for AM2.

Pores cannot be responsible for the comparatively high roughness of the micromilled reference workpieces. The similar roughness of the reference material and AM1 is caused by the similar cutting edge wear. Both cutting edges of the micromilling tools used when milling AM1 and the reference show hardly any wear compared to those of AM2. As a result, the kinematic roughness is reduced to a lower extent compared to AM2, which leads to a higher arithmetic average profile roughness.

In Fig. 8c, the arithmetical mean height Sa for AM1, AM2, and the reference material is shown for both feed directions. Since the minimum chip thickness is not reached throughout the whole width of the groove, plowing is increased in the outer area which leads to deviations between the surface of the groove's center and the groove's edge. Since Sa is an areal roughness parameter, it is also influenced by the area near the groove's edge. This surface-based calculation results in differences between Ra and Sa values. Contrary to the conclusions of Fig. 8a and b, micromilling of the reference material reaches the lowest values of roughness when considering Sa. This result may be attributed to the more regular and non-porous structure of the reference material.

3.2.4 Burr formation

Figure 9 shows the SEM images of the milled structures at a feed travel of $l_f = 320–340$ mm for AM1 and AM2 with feed direction parallel and perpendicular to their build-up direction.

Regarding the burr formation, differences caused by varying feed direction and machined material are apparent when machining AM workpieces. When considering all combinations of feed direction and workpiece, a significant difference in the amount of burr formation between down and up milling can be seen. The burr formation during down milling is much stronger compared to up milling. Further, the amount of burr formation on the down milling side of AM1 and AM2 machined parallel to the build-up direction is very similar.

The different degrees of burr formation depending on the feed direction are again a result of the characteristic microstructure of the AM workpieces. As the micromilling tool moves through the material, a chip whose maximum thickness corresponds to the feed per tooth, is separated. At the edges of the grooves, the chip is not separated and reams as burr since the minimum chip thickness is not reached any more. The different degrees of burr formation thus indicate differences in the length of the not separated chips. These differences in length match the determined melt path dimensions w and h of AM1 and AM2 in combination with the kinematics of the milling process. During machining with feed direction parallel to the build-up direction, the micromilling tool separates a chip along the melt path's width w, which, due to $w/h > 1$ applying for all AM workpieces, results in a longer chip and thus in increased burr formation due to not separating the chip at the groove's edge. The reduced burr formation during machining with feed direction perpendicular to the build-up direction is therefore due to the separation of the chips along the melt path's height h, which is typically smaller than w. The difference in the degree of the direction-dependent burr formation is again due to the different ratios of w/h of AM1 and AM2, significantly influencing the melt path's dimensions. This is confirmed when arranging the amount of burr formation in an increasing order, correlating exactly with the determined melt path dimensions: AM2 machined perpendicular to the build-up direction ($h_{AM2} = 41$ µm), AM1 machined perpendicular to the build-up direction ($h_{AM1} = 51$ µm), AM1 machined parallel to the build-up direction ($w_{AM1} = 73$ µm), and AM2 machined parallel to the build-up direction ($w_{AM2} = 84$ µm).

Figure 10 shows the SEM images of the milled structures at a feed travel of $l_f = 320–340$ mm for the reference material.

The formation of burrs when machining the reference material is strong although the tool does not pass any melt paths. The deviating structure at the edge of the groove bottom is due to the wear of the cutting edge of the micromilling tools.

4 Conclusion and outlook

This paper focuses on the effects of the process parameters of additive manufacturing on the generated workpiece properties as well as on the subsequent micromilling process. Two types of workpieces, differing in relative density and microhardness (AM1 and AM2), were produced using different combinations of process parameters for selective laser melting.

The generated workpieces were characterized regarding their chemical composition, as-built surface roughness, hardness, relative density, and melt path geometry. When micromilling, the feed direction was varied in dependence of the build-up direction of the additively manufactured workpieces. The feed direction was classified as perpendicular to the build-up direction and parallel to the build-up direction. The effects of the difference in workpiece production and feed directions on the micromilling process and its results were shown on the basis of process forces, surface roughness of the machined surface, tool wear, and burr formation. The results of AM1 and AM2 were compared with those of casted, rolled, solution-annealed, and water-quenched reference material.

The investigations of micromilling showed significant differences when varying the feed direction in relation to the build-up direction, which was attributed to the characteristic microstructure of workpieces manufactured by selective laser melting.

The analysis of the roughness of the machined surfaces showed differences between AM1 and AM2, due to the low

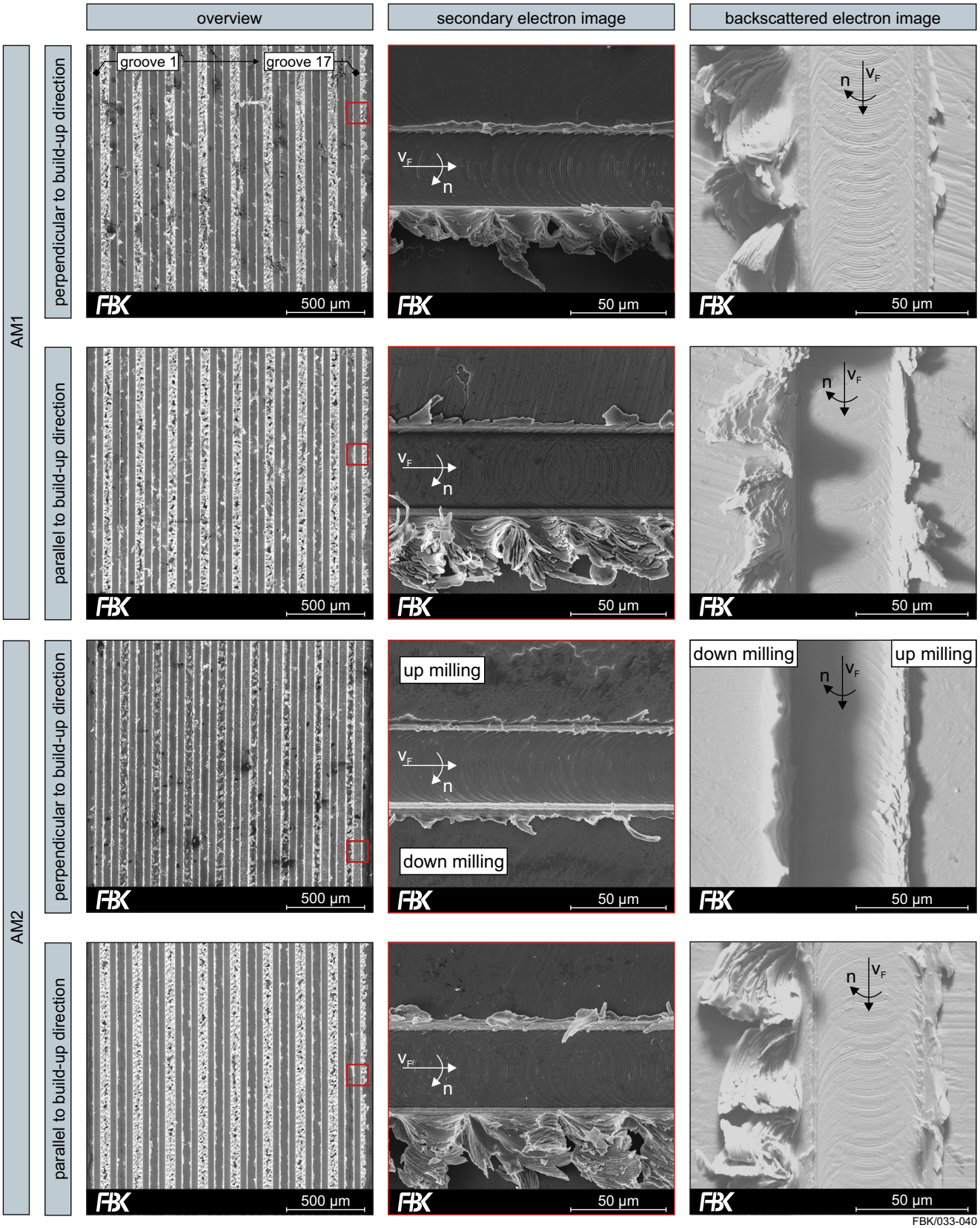

Fig. 9 Burr formation during machining of AM1 and AM2 parallel and perpendicular to the build-up direction

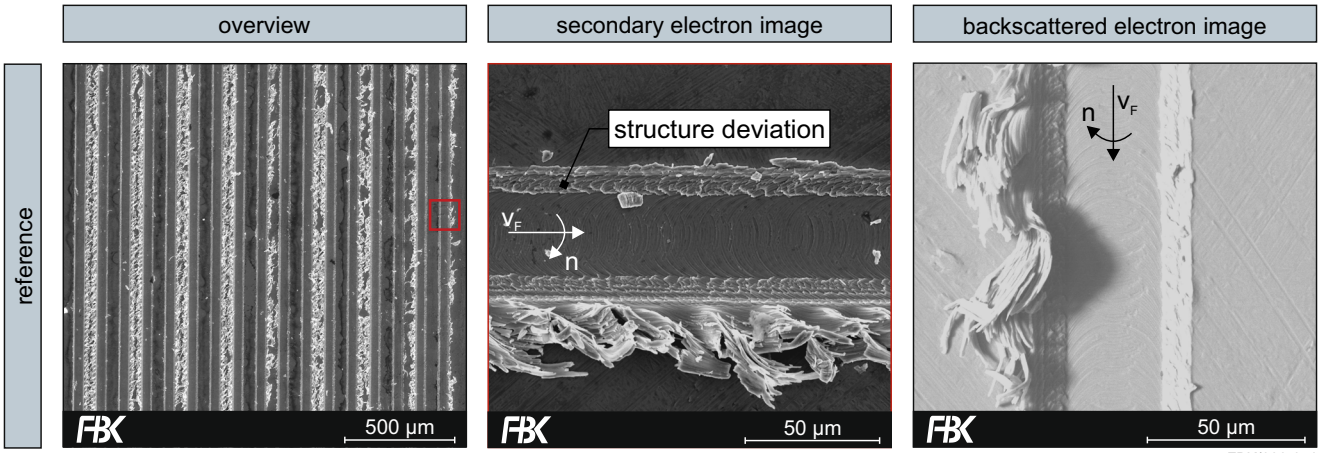

Fig. 10 Burr formation during machining of the reference material

relative density of AM1. The surface roughness inside open pores was determined to be significantly higher than those of the surrounding milled structures, leading to an increased surface roughness of more porous workpieces.

The wear behavior of the micromilling tools corresponded to the process forces and showed dependencies on material and feed direction. The largest tool wear was determined for AM2 workpieces as the increased relative density of AM2 results in a higher material removal. The analysis of the process forces showed a rather continuous increase during machining of the reference workpieces, whereas tools used for AM2 tend towards increased formation of built-up edges. The absolute values of the process forces during machining of AM workpieces were attributed to the crossing of melt borders. Further, the differences in process force were related to the melt path width and height of the AM workpieces, defined during SLM.

The burr formation was also influenced by the dimensions of the melt paths of the AM workpieces. The influence of the feed direction was attributed to the direction of chip separation. The degree of burr formation is dependent on the melt path width and height of AM workpieces.

In further investigations, more process parameters for SLM will be investigated, varying the layer thickness and hatch spacing, resulting into different ratios of melt path width to height. By using these new process parameters and by applying heat treatments, the effects of the anisotropic material structure on the tool wear, process forces, burr formation, and roughness shown in this paper will be confirmed.

Authors' contributions Sebastian Greco: investigation, data curation, visualization, writing of original draft.

Sonja Kieren-Ehses: investigation, writing, reviewing, and editing.

Benjamin Kirsch: supervision, writing, reviewing, and editing.

Jan C. Aurich: project administration, supervision, writing, reviewing, and editing.

Funding Open Access funding enabled and organized by Projekt DEAL. The authors would like to thank the German Research Foundation (DFG) for the financial support within the project AU 185/57-1 "Ultrasonic air bearing spindle for micro machining." Also funded by the Deutsche Forschungsgemeinschaft (DFG, German Research Foundation) (project ID 172116086–SFB 926). Open Access funding provided by Projekt DEAL.

Data availability The datasets generated during and/or analyzed during the current study are available from the corresponding author on reasonable request.

Compliance with ethical standards

Competing interests The authors declare that they have no competing interests.

Disclaimer [1]Naming of specific manufacturers is done solely for the sake of completeness and does not necessarily imply an endorsement of the named companies nor that the products are necessarily the best for the purpose.

References

1. Riveiro A, del Val J, Comesaña R, Lusquiños F, Quintero F, Boutinguiza M, Pou J (2019) Laser additive manufacturing processes for near net shape components. Near Net Shape Manufacturing Processes:105–141

2. Kleer R, Piller FT (2019) Local manufacturing and structural shifts in competition: market dynamics of additive manufacturing. Int J Prod Econ 216:23–34
3. Islam M, Purtonen T, Piili H, Salminen A, Nyrhilä O (2013) Temperature profile and imaging analysis of laser additive manufacturing of stainless steel. Phys Procedia 41:835–842
4. Nagarajan B, Hu Z, Song X, Zhai W, Wei J (2019) Development of micro selective laser melting: the state of the art and future perspectives. Engineering 5:702–720
5. Peng T, Chen C (2018) Influence of energy density on energy demand and porosity of 316L stainless steel fabricated by selective laser melting. International Journal of Precision Engineering and Manufacturing-Green Technology 5(1):55–62
6. Li R, Liu J, Shi Y, Wang L. Balling behavior of stainless steel and nickel powder during selective laser melting process. Int J Adv Manuf Technol 2012; 59.9–5912; 1025–1035
7. Silva M, Felismina R, Mateus A, Parreira P, Malça C (2017) Application of a hybrid additive manufacturing methodology to produce a metal/polymer customized dental implant. Procedia Manufacturing 12:150–155
8. Fischer J, Kniekamp M, Abele E. Micro laser melting: analyses of current potentials and restrictions for the additive manufacturing of micro structures. Proceedings of the 25th Annual International Solid Freeform Fabrication Symposium 2014; 22–35
9. Gieseke M, Senz V, Vehse M, Fiedler S, Irsig R, Hustedt M, Sternberg K, Nölke C, Kaierle S, Wesling V, Tiggesbäumker J, Meiwes Broer KH, Seitz H, Schmitz KP, Haferkamp H. Additive manufacturing of drug delivery systems. Biomedical Engineering/ Biomedizinische Technik 2012; 57/SI-1 Track-S; 398–401
10. Noelke C, Gieseke M, Kaierle S. Additive manufacturing in micro scale. International Congress on Applications of Lasers & Electro Optics 2013; 2013/1; 1–6
11. Coelho R, Azevedo R, Assis C. An investigation of anisotropy on AISI 316L obtained by additive manufacturing (AM) measuring surface roughness after micro-endmilling operations. Proceedings of the 18th euspen International Conference 2018; 357–358
12. Kaynak Y, Kitay O. Porosity, surface quality, microhardness and microstructure of selective laser melted 316L stainless steel resulting from finish machining. Journal of Manufacturing and Materials Processing 2018; 2/2; 36
13. Alexeev VP, Balyakin AV, Khaimovich AI. Influence of the direction of selective laser sintering on machinability of parts from 316L. IOP Conference Series: Materials Science and Engineering 2017; 177/1; 012120
14. Cheng K, Huo D (2013) Micro-cutting: fundamentals and applications. John Wiley & Sons
15. Riley NA. Projection sphericity. Journal of Sedimentary Research 1941, 11/2, 94–95
16. Greco S, Gutzeit K, Hotz H, Kirsch B, Aurich JC. Selective laser melting (SLM) of AISI 316L – impact of laser power, layer thickness, and hatch spacing on roughness, density, and microhardness at constant input energy density. The International Journal of Advanced Manufacturing Technology 2020, 108/5–6, 1551–1562
17. Sinicio M, Witvrouw A, Dewulf W (2019) Influence of the particle size distribution on surface quality of Maraging 300 parts produced by laser powder bed fusion. Proceedings of the Special Interest Group meeting on Advanced Precision in Additive Manufacturing: 31–34
18. Bohley M, Reichenbach IG, Müller C, Aurich JC. Development of a desktop machine tool for integrated ultra-small micro end mill production and application. Proceedings of the 11th International Conference on Micromachining 2016; 29–31
19. Bohley M, Kieren-Ehses S, Kirsch B, Aurich JC (2017) Die gesamte Prozesskette der Mikrofräsbearbeitung. Mav - Innovation in der spanenden Fertigung 11:18–21
20. Aurich JC, Reichenbach IG, Schüler GM. Manufacture and application of ultra-small micro end mills. CIRP annals 2012, 61/1, 83–86
21. Bohley M, Reichenbach IG, Müller C, Aurich JC. Development of a desktop machine tool for integrated ultra-small micro end mill production and application. Proceedings of the 11th International Conference on Micro Manufacturing 2016, 13, 1–6
22. Reichenbach IG, Aurich JC (2013) Untersuchung der Oberflächengüte beim Mikrofräsen – Einfluss von Prozessparametern und Einstellwinkel der Nebenschneide bei 48 μm Mikroschaftwerkzeugen. Wt Werkstatttechnik Online 103:11–12
23. DIN. DIN EN ISO 4288, Geometrische Produktspezifikationen (GPS) - Oberflä-chenbeschaffenheit: Tastschnittverfahren - Regeln und Verfahren für die Beurteilung der Oberflächenbeschaffenheit. Berlin: Beuth Verlag, 1997
24. Aurich JC, Greco S, Hotz H, Zimmermann M, Hartig J, Kirsch B. Schleifende Nachbearbeitung additiv gefertigter austenitischer Edelstähle. ZWF - Zeitschrift für wirtschaftlichen Fabrikbetrieb 2017, 7/8, 473–476
25. Vogel H (1997) Gerthsen Physik. Springer
26. Yap CY, Chua CK, Dong ZL, Liu ZH, Zhang DQ, Loh LE, Sing SL. Review of selective laser melting: materials and applications. Applied physics reviews 2018, 2/4, 041101
27. Kamath C, El-dasher B, Gallegos GF, King WE, Sisto A. Density of additively-manufactured, 316L SS parts using laser powder-bed fusion at powers up to 400 W. The International Journal of Advanced Manufacturing Technology 2014, 74/1–4, 65–78
28. Rai R, Elmer JW, Palmer TA, DebRoy T. Heat transfer and fluid flow during keyhole mode laser welding of tantalum, Ti–6Al–4V, 304L stainless steel and vanadium. Journal of physics D: Applied physics 2007, 40/18, 5753
29. Yusuf SM, Chen Y, Boardman R, Yang S, Gao N. Investigation on porosity and microhardness of 316L stainless steel fabricated by selective laser melting. Metals 2017; 7/2; 64
30. Ma M, Wang Z, Zeng X (2017) A comparison on metallurgical behaviors of 316L stainless steel by selective laser melting and laser cladding deposition. Mater Sci Eng A 685:265–273
31. Vilaro T, Colin C, Bartout JD, Nazé L, Sennour M (2012) Microstructural and mechanical approaches of the selective laser melting process applied to a nickel-base superalloy. Mater Sci Eng A 534:446–451
32. Popov KB, Dimov SS, Pham DT, Minev RM, Rosochowski A, Olejnik L. Micromilling: material microstructure effects. Proceedings of the Institution of Mechanical Engineers, Part B: Journal of Engineering Manufacture 2006, 220/11, 1807-1813
33. Attanasio A, Gelfi M, Pola A, Ceretti E, Giardini C. Influence of material microstructures in micromilling of Ti6Al4V alloy. Materials 2013, 6/9, 4268–4283
34. Hall EO. The deformation and ageing of mild steel: III discussion of results. Proceedings of the Physical Society. Section B 1951; 64.9; 747–753
35. Oettel H, Schumann H (Eds.). Metallografie: mit einer Einführung in die Keramografie. John Wiley & Sons 2011